

AG

503543



STATE RESEARCH CENTER OF RUSSIA  
INSTITUTE FOR HIGH ENERGY PHYSICS



IHEP 95-50

V.B. Anikeev, S.V. Belikov, A.A. Borisov, N.I. Bozhko, S.K. Chernichenko,  
V.N. Goryachev, S.N. Gurgiev, M.M. Kirsanov, A.I. Kononov, A.S. Kozhin,  
V.I. Kravtsov, V.A. Kulikov, V.V. Lipaev, A.I. Mukhin, S.A. Mukhin,  
V.F. Perelygin, Yu.I. Salomatin, Yu.I. Sapunov, A.V. Sidorov,  
A.A. Spiridonov, Yu.M. Sviridov, V.V. Sytnik, K.E. Shestermanov,  
G.L. Schukin, V.L. Tumakov, A.S. Vovenko, V.P. Zhigunov  
*Institute for High Energy Physics, Protvino, Russia*  
L.S. Barabash, S.A. Baranov, Yu.A. Batusov, S.A. Bunyatov, O.A. Denisov,  
A.G. Karev, M. Yu. Kazarinov, O.L. Klimov, V.V. Lyukov, Yu.A. Nefedov,  
S.N. Prakhov, V.I. Snyatkov, A.A. Vovenko  
*Joint Institute for Nuclear Research, Dubna, Russia*

**TOTAL CROSS SECTION MEASUREMENTS  
FOR  $\nu_\mu, \bar{\nu}_\mu$  INTERACTIONS IN 3–30 GeV ENERGY RANGE  
WITH IHEP–JINR NEUTRINO DETECTOR**

Submitted to "Zeitschrift für Physik C"

Protvino 1995

**Abstract**

Anikeev V.B. et al. Total cross section measurements for  $\nu_\mu, \bar{\nu}_\mu$  interactions in 3 – 30 GeV energy range with IHEP–JINR Neutrino Detector: IHEP Preprint 95-50. – Protvino, 1995. – p. 18, figs. 10, tables 5, refs.: 46.

The results of total cross section measurements for the  $\nu_\mu, \bar{\nu}_\mu$  interactions with isoscalar target in the 3 – 30 GeV energy range have been presented. The data were obtained with the IHEP–JINR Neutrino Detector in the "natural" neutrino beams of the U-70 accelerator. Neutrino fluxes were obtained by averaging the spectra, based on the calculations with the use of the experimental data on secondary particle yields from the target and muon fluxes measurements in 9 gaps of the muon filter, as well as the spectra determined from quasielastic events and spectra defined by extrapolating differential distribution  $\frac{d\sigma}{dy}$  in the region  $y = 0$ . The significant deviation from the linear dependence for  $\sigma_{tot}$  versus neutrino energy is determined in the energy range less than 15 GeV.

**Аннотация**

Аникеев В.Б. и др. Определение полных сечений нейтрино и антинейтрино на нуклоне в области 3-30 ГэВ на Нейтринном Детекторе ИФВЭ-ОИЯИ: Препринт ИФВЭ 95-50. – Протвино, 1995. – 18 с., 10 рис., 5 табл., библиогр.: 46.

В работе представлены результаты измерения полных сечений взаимодействия  $\nu_\mu, \bar{\nu}_\mu$  на изоскалярной мишени в области энергий нейтрино от 3 до 30 ГэВ. Данные были получены на Нейтринном Детекторе ИФВЭ-ОИЯИ в "естественных" пучках нейтрино ускорителя У-70. Нейтринные потоки определялись усреднением спектров, полученных на основании расчетов, использующих данные по выходам  $\pi, K$ -мезонов с мишени, и измерений мюонных потоков в 9 разрезах мюонного фильтра, а также спектров, определенных по квазиупругим событиям и полученных экстраполяцией дифференциального распределения  $\frac{d\sigma}{dy}$  в область  $y = 0$ . Установлено существенное отклонение в области энергий меньшей 15 ГэВ от линейной зависимости  $\sigma_{tot}$  от энергии нейтрино.

## Introduction

Many experimental results on measuring the total cross section of the charged current neutrino and antineutrino interactions on nucleon have been published (table 1). The accurate data [1],[2],[3] obtained in the  $30 \text{ GeV} < E_\nu < 200 \text{ GeV}$  energy range give evidence for the cross section linear dependence versus the energy in this range. In the framework of the naive quark-parton model the slope parameter  $\sigma_{tot}/E_\nu$  in the deep inelastic region is independent of the energy, with the exception of possible threshold effects caused by charm particles production. In the range  $E_\nu < 20 \text{ GeV}$  systematic measurements are lacking and available experimental data have considerable errors. Note, that the trend has been observed towards neutrino cross section slope growth with the decrease of neutrino energy, although some experimental data contradict this assertion. To make more precise measurements in the low energy range the experiment with the Neutrino Detector (ND) [15] was carried out.

The experimental results for  $\sigma_{tot}$  measurement in "natural" (without using a focusing device) wide band neutrino beams of the U-70 accelerator are presented. Experimental data have been obtained for two ND expositions:

- 1) conventional geometry of the neutrino channel with the focusing system off (fig.1);
- 2) with short decay base neutrino channel, optimized for the search for  $\nu_\epsilon \rightarrow \nu_x$  oscillations without the use of the focusing device for the neutrino beam formation. The used types of the neutrino beam with some statistics losses as compared to the focused neutrino beam mode allow one to diminish the systematic errors in calculating neutrino and antineutrino spectra due to uncertainties with account of the focusing device influence on  $\pi$ ,  $K$ -mesons. A possibility to detect neutrino and antineutrino events simultaneously excludes some sources of systematic errors in determining the energy dependence of the total cross section ratio for neutrino and antineutrino, such as an uncertainty in the proton beam intensity monitoring and that of detector efficiency due to the variation in background conditions and calibration parameters of tracking detectors.

Table 1. The published experimental data of the neutrino and antineutrino total cross section.

	E, GeV	$\sigma_{tot}/E \times 10^{-38} \text{cm}^2/\text{GeV}$		
$\nu$	20-200	$0.67 \pm 0.02$	CCFR, CDHSW, CHARM	[1],[2],[3]
$\nu$	3	$0.79 \pm 0.15$	BNL (1980)	[4]
	9	$0.75 \pm 0.23$		
$\nu$	1	$0.96 \pm 0.06$	BNL (1981)	[5]
	9	$0.80 \pm 0.03$		
$\nu$	3.6	$0.62 \pm 0.09$	GGM(1973)	[6]
	3.8	$0.79 \pm 0.11$		
	4.5	$0.66 \pm 0.07$		
	5.5	$0.96 \pm 0.13$		
	6.5	$1.09 \pm 0.19$		
	7.5	$1.08 \pm 0.20$		
	8.5	$0.86 \pm 0.19$		
$\nu$	2.87	$0.69 \pm 0.05$	GGM(1979)	[8]
	9.05	$0.61 \pm 0.06$		
$\nu$	15	$0.57 \pm 0.07$	GGM(1981)	[9]
	22	$0.55 \pm 0.07$		
	26	$0.63 \pm 0.07$		
$\nu$	17	$0.75 \pm 0.11$	BEBC(1979)	[10]
	34	$0.73 \pm 0.10$		
$\nu$	3-5	$0.68 \pm 0.07$	SKAT(1979)	[11]
	5-9	$0.70 \pm 0.09$		
	9-16	$0.86 \pm 0.13$		
$\nu$	5-8	$0.77 \pm 0.04$	IHEP-ITEP(1979)	[12]
	8-12	$0.74 \pm 0.04$		
	12-20	$0.72 \pm 0.04$		
	20-35	$0.68 \pm 0.06$		
$\nu$	0.5-2	$0.96 \pm 0.06$	ANL(1979)	[13]
$\bar{\nu}$	20-200	$0.33 \pm 0.02$	CCFR, CDHSW, CHARM	[1],[2],[3]
$\bar{\nu}$	1-8	$0.26 \pm 0.02$	GGM(1979)	[7]
$\bar{\nu}$	7	$0.30 \pm 0.02$	GGM(1981)	[9]
	9	$0.31 \pm 0.04$		
	25	$0.32 \pm 0.07$		
$\bar{\nu}$	28	$0.32 \pm 0.07$	BEBC(1979)	[10]
$\bar{\nu}$	5-8	$0.30 \pm 0.02$	IHEP-ITEP(1979)	[12]
	8-12	$0.31 \pm 0.04$		
	12-20	$0.32 \pm 0.05$		
	20-35	$0.32 \pm 0.07$		

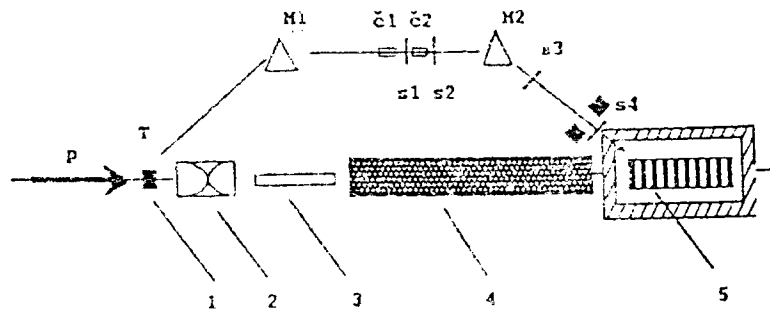


Fig. 1. The neutrino channel scheme: 1 - target, 2 - focusing device, 3 - decay pipe, 4 - muon filter, 5 - neutrino detector. M1-M2 - deflecting magnets, Č1 - Č2 - Cerenkov counters, S1-S2 - scintillation counters.

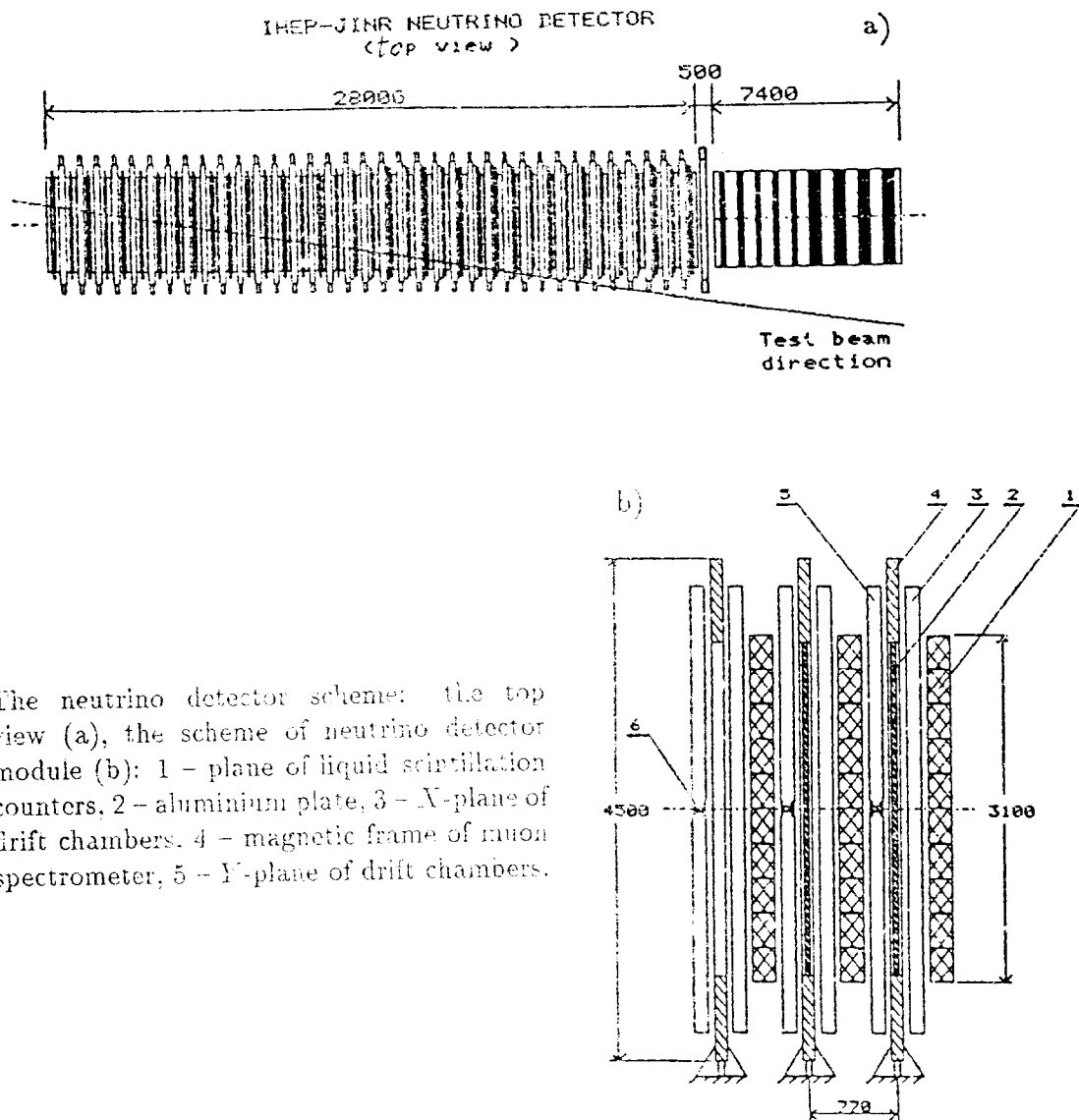


Fig. 2. The neutrino detector scheme: the top view (a), the scheme of neutrino detector module (b): 1 - plane of liquid scintillation counters, 2 - aluminium plate, 3 - X-plane of drift chambers, 4 - magnetic frame of muon spectrometer, 5 - Y-plane of drift chambers.

# 1. Experimental Setup

The Neutrino Detector of IHEP-JINR Collaboration is located in the neutrino channel [16] at 223 m from aluminium target 60 cm long and 10 mm in diameter. The decay tunnel is 140 m long, followed by 55 m of steel to absorb the muons. The ionization chambers were placed in 9 gaps of the muon filter to measure muon flux topography [17]. These measurements were used as additional information to determine neutrino fluxes through ND.

For the neutrino beam formation in the neutrino channel with short decay base the aluminium target 60 mm in diameter and 60 cm in length was placed at about 70 m before ND. The decay volume inside the steel shield behind the target looked like the taper cavity 12.1 m long with rectangular cross section.

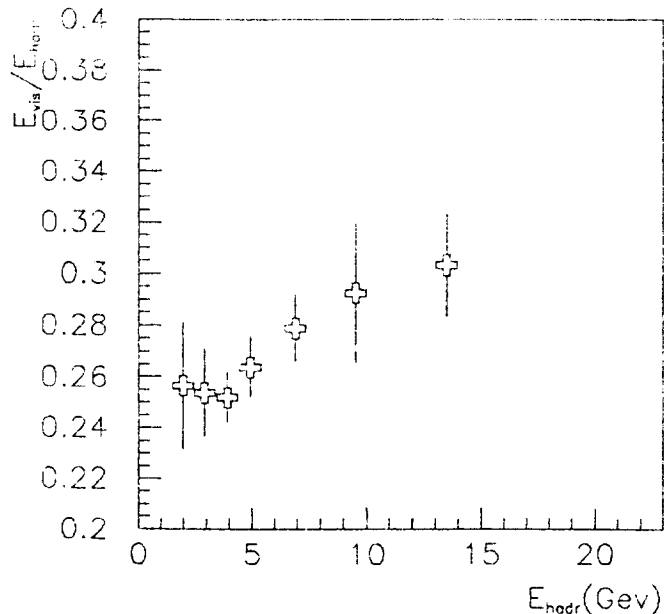
The intensity and the proton beam profiles on the neutrino target were controlled by current transformers with 1% accuracy. Average intensity of the proton beam was  $\approx 10^{13}$  protons per 9 seconds accelerator spill.

The neutrino detector is a calorimeter mounted inside the magnetized steel muon spectrometer. The target-calorimeter (fig.2) contains 36 planes of horizontally mounted liquid scintillation counters [19] of 20 cm (along the beam)  $\times$  30 cm size and 500 cm long, interleaved with 5 cm thick aluminium plates of  $3 \times 3$  m<sup>2</sup> area. These plates are mounted into the magnetized steel frames. The  $X$ - and  $Y$ -planes of vector drift chambers [18] are placed between scintillation counters planes and aluminium filters. Drift chambers cover the area  $450 \times 450$  cm<sup>2</sup> and detect particles in the target part and muons passing through the steel frames, which are the magnetic shell of the muon spectrometer. The end-cap part of the muon spectrometer consists of 13 magnetized steel toroidal disks 22 cm thick and 4 m in diameter with drift chamber planes placed between them. The muon spectrometer was focusing  $\mu^-$ , but the detector efficiency of  $\mu^+$  in the magnetic shell was high as well.

The information readout was organized without trigger, the detector data acquisition starts after the proton beam fast spill signal arrives. During the 12  $\mu$ s time interval, which is equal to the sum of 5  $\mu$ s beam spill duration and 7  $\mu$ s maximal electron drift time in the chambers, the amplitude and time information from scintillation counters and time information from drift chambers were registered.

For calibration [23] the test channel was used (fig.1). Charged particles were by-passed over the shield and muon filter of the neutrino channel and then were directed into the detector. The system of deflecting magnets, collimators, Cerenkov and scintillation counters allows one to select particles with momentum spread within 0.7%. As a result of calorimeter calibration with  $\pi^-$ -mesons test beam, the dependence of the relative energy deposition coefficient  $\alpha = E_{vis}/E_{hadr}$  versus  $E_{hadr}$  was defined (fig.3), which was used in the hadron shower energy determination. The energy resolution of the calorimeter for hadron energy deposition can be presented as  $\sigma(E_h)/E_h = 39.5\%/\sqrt[3]{E_h}(\text{GeV})$ .

Fig. 3. The dependence of the relative energy deposition coefficient for hadron shower  $\alpha = E_{vis}/E_{hadr}$  versus hadron energy  $E_{hadr}$ .



The test beam also contained a small fraction of muons, which were used to test the muon momentum reconstruction in the detector. The accuracy of the muon momentum reconstruction corresponds to the physical characteristics of the magnetic system and mainly depends on the track length in the magnetic field. For the tracks with the maximal length in the magnetized steel of the muon spectrometer, the momentum measurement error is 12% for 5 GeV and it increases up to 20 % for 30 GeV muons due to drift chamber spatial resolution [24].

## 2. Data Processing

Detected events having different interaction time or coordinate position were separated by the off-line program GRAND [24], based on the algorithms using the scintillation counters information. For each event with a muon in the final state the energy and angle of the hadron shower as well as [20]) the muon sign and momentum were determined. In 9% of the reconstructed muon with determined sign on condition that the track in the magnetic field was short, the momentum was calculated on the base of the measured hadron energy and muon and hadron angles from the vertex. The calculated value of the neutrino energy as a sum of the muon momentum and hadron shower energy was corrected by procedure of the kinematic fit [21] based on the 4-momentum conservation by .

With account for the detector acceptance, its smearing and detection efficiency for each of two types of neutrino beam  $1.2 \cdot 10^5 \nu$  and  $2 \cdot 10^4 \bar{\nu}$  events were generated with the interaction vertex in the  $260 \times 260 \times 2550 \text{ cm}^3$  volume of the ND target part. Simulated events were obtained with program CATAS [32] in assumption of Feynman-Field parameterization [33] for quark distributions with linear dependence of the total cross section versus energy. If the invariant mass  $W$  of the hadron system was less then 2 GeV, then

Rein-Seghal model [34] was used to describe the interaction in this  $W$  range by means of the nucleon resonance production set. The quasielastic interactions were simulated according to [35], where the values of axial and vector formfactors  $M_A = 1.00 \text{ GeV}/c^2$  and  $M_V = 0.84 \text{ GeV}/c^2$  were used.

Simulated data were modified to the same format as that of the experimental information: digitizing from TDC and ADC for liquid scintillation counters and digitizing from TDC for drift chambers. During this procedure the detector background, obtained from the real experimental data after having removed the information about the neutrino interactions, was added to generated neutrino events. Then the obtained data were processed with the same event reconstruction program GRAND, which was applied to experimental events.

Detection inefficiency of the neutrino events mainly caused by the fact that some fraction of muons has the energy insufficient for the detection ( $E_\mu < 1 \text{ GeV}$ ), and the other fraction of muons with large angles in the vertex ( $20 - 30^\circ$ ) had bad conditions to be detected in the muon spectrometer. In fig.4 the dependence of the muon momentum and sign reconstruction efficiency (on condition that the track crosses more than 3 magnetic modules) versus the angle is shown. The muon intersection with the hadron shower can also result in muon loss. Since the products of neutrino interactions in ND in the surrounding matter sometimes overlap an additional difficulty in the muon recognition arises. Simulation takes into account these effects, and the number of the reconstructed events decreases by the value of  $10 \pm 2\%$ . no correlation between any physical parameters of the event (neutrino energy, muon momentum, hadron energy,  $Q^2$ , scaling variables  $X, Y$ ) has been observed. Fig.5 presents efficiencies to select neutrino and antineutrino events for the further physical analysis according to the criteria, described below, as a function of energy.

### 3. Measurement of Total Cross Section Energy Dependence

#### 3.1. Neutrino Events Selection

For physical analysis only that part of statistics was selected, for which the proton beam intensity was reliably measured and the monitoring system provided precise beam position on the target. For the exposition with the conventional geometry the number integrated protons, was  $1.09 \times 10^{18}$  and for the exposition with short decay base it was  $1.68 \times 10^{18}$  protons.

To exclude the events induced by the products of neutrino interaction in the muon filter, the events with vertex in the first 3 modules were not used. The events with vertex in the last 6 modules were also rejected. The fiducial volume has transverse dimensions  $240 \times 240 \text{ cm}^2$  and total weight 55.6 tons. If muon momentum was calculated by the track curvature in the magnetic field, the length of the muon track in the magnetic field was required to satisfy the condition  $l_{mag} > 30 \text{ cm}$ . To decrease a contribution of neutrino events in the antineutrino sample  $l_{mag}$  was to be  $> 50 \text{ cm}$ . The measured energy of neutrino interaction was to be in the range  $3 \text{ GeV} < E_\nu < 30 \text{ GeV}$  as well.



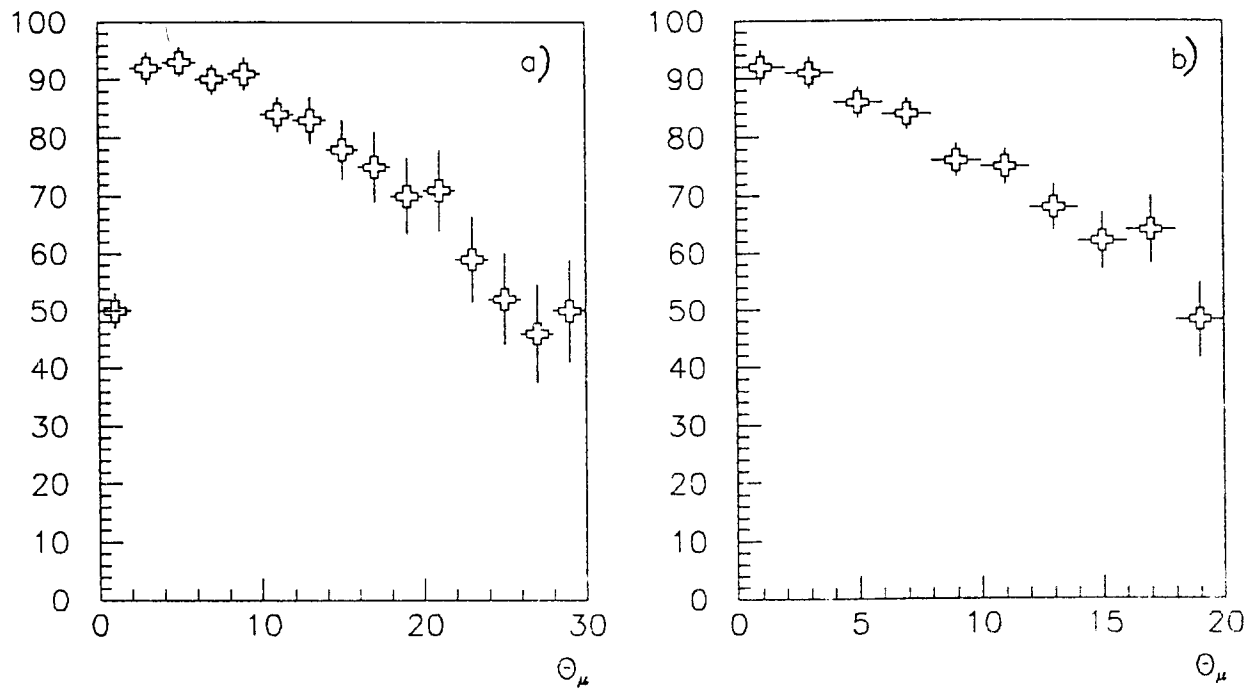
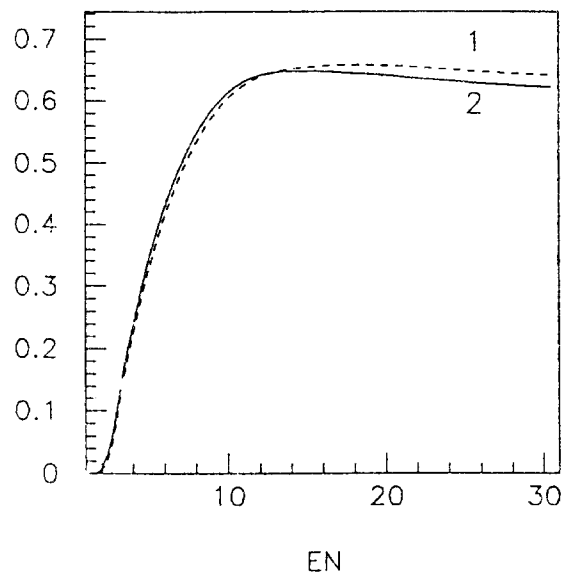


Fig. 4. The dependence of muon sign (a) and momentum reconstruction efficiency (b) versus muon angle.

Fig. 5. The dependence of neutrino event reconstruction efficiency versus energy: 1 - neutrino, 2 - antineutrino.



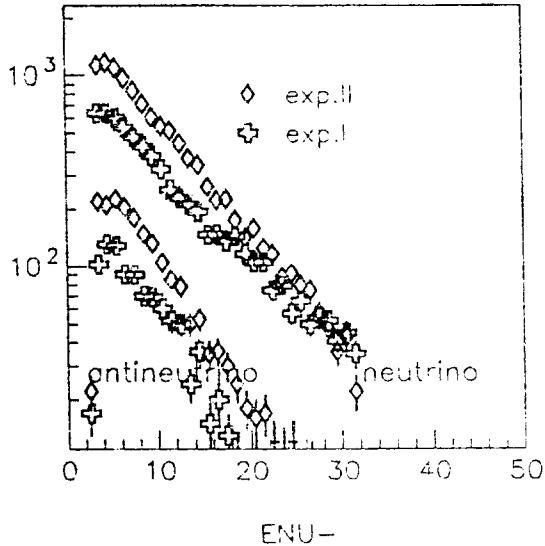


Fig. 6. Distributions of registered neutrino and antineutrino events in the exposition with the conventional geometry (1) and with short decay base (2).

After above-mentioned cuts 6376  $\nu$ , 1045  $\bar{\nu}$  events in the first exposition and 10690  $\nu$ , 1934  $\bar{\nu}$  in the second one have been obtained. Their energy distributions are shown in fig.6. The neutrino energy distributions for initially selected events  $N_0$  and those, obtained after the subtraction of the background events from the neutral current interaction and the events with wrong muon sign (the value  $N$  in Tables), as well as the corrected distribution of the events  $N_{cor}$  obtained with the procedure, described below, that takes into the account the detector smearing, are presented in Tables 2 and 3 for each exposition.

### 3.2. Energy Spectra Determination for Neutrino and Antineutrino Fluxes

The experimental data [25] for secondary particles yields from long targets, used for neutrino beam calculation, have been taken. The program GEASPE [30], based on the GEANT [31] library was used in calculation. The program allows one to take into account hadron showering in the substance and particles over-scattering in the walls of the decay tunnel. As a result of the program processing, the obtained two-dimensional (energy-radius or energy-angle) distribution for the neutrino flux was used as an input information in simulating neutrino events in the detector.

Calculated neutrino and antineutrino fluxes passing through the fiducial volume of the detector, obtained by means of the GEASPE program, are shown on fig.7.

Based on the experimental data for  $\pi$ ,  $K$ -mesons yields muon fluxes in the gaps of the muon filter (fig.8) were simulated by the same program. As the muon flux in the shield is directly associated with neutrino flux [27],[28], from the comparison of experimental muon fluxes (which were measured with an accuracy of  $\approx 3\%$  [29]) and calculated fluxes it is possible to make a conclusion that in the region of neutrino energy up to 20 GeV the accuracy of the calculated neutrino fluxes is not worse than 5%, but in the region from 20 to 30 GeV it is 10-15% due to  $K/\pi$  ratio.

Table 2. The energy distributions of neutrino and antineutrino interaction events, the value of the total cross section slope, statistical and systematic errors in exposition with neutrino channel conventional geometry.

		neutrino								
$E_\nu$ [GeV]		3-5	5-7	7-9	9-11	11-13	13-17	17-21	21-25	25-30
$N_0$		652	1236	1014	806	578	783	543	364	227
$N$		626.0	1192.0	981.4	771.3	564.2	768.5	530.8	353.0	218.0
$N_{cor}$		691.7	1086.9	941.1	733.9	563.5	788.1	514.9	361.5	237.0
$\sigma_{tot}/E_\nu$		0.746	0.822	0.790	0.756	0.731	0.698	0.671	0.655	0.617
$\Delta_{stat}$		0.030	0.024	0.026	0.028	0.031	0.025	0.030	0.034	0.040
$\Delta_{\Sigma sys}$		0.057	0.050	0.050	0.037	0.038	0.041	0.042	0.058	0.078
		antineutrino								
$E_\nu$ [GeV]		3-5	5-7	7-10	10-13	13-17	17-21	21-26	26-30	
$N_0$		104	264	247	176	124	51	47	31	
$N$		96.5	251.6	231.8	155.3	112.7	40.4	39.7	23.9	
$N_{cor}$		121.9	207.1	234.4	155.1	112.5	53.7	38.8	23.5	
$\sigma_{tot}/E_\nu$		0.333	0.353	0.337	0.368	0.346	0.283	0.268	0.304	
$\Delta_{stat}$		0.027	0.019	0.016	0.020	0.023	0.031	0.038	0.054	
$\Delta_{\Sigma sys}$		0.034	0.030	0.029	0.034	0.053	0.032	0.034	0.050	

Table 3. The energy distributions of neutrino and antineutrino interaction events, the value of the total cross section slope, statistical and systematic errors in the oscillation experiment with short decay base.

		neutrino								
$E_\nu$ [GeV]		3-5	5-7	7-9	9-11	11-13	13-17	17-21	21-25	25-30
$N_0$		1141	2252	1797	1318	1060	1415	766	488	305
$N$		1102.9	2026.6	1762.3	1296.7	1048.9	1398.1	757.6	484.9	303.0
$N_{cor}$		1245.9	1991.1	1690.4	1287.9	1001.9	1370.4	798.5	505.1	303.3
$\sigma_{tot}/E_\nu$		0.813	0.812	0.764	0.717	0.699	0.667	0.636	0.616	0.602
$\Delta_{stat}$		0.020	0.016	0.018	0.020	0.022	0.019	0.025	0.032	0.041
$\Delta_{\Sigma sys}$		0.081	0.074	0.075	0.050	0.051	0.050	0.052	0.059	0.074
		antineutrino								
$E_\nu$ [GeV]		3-5	5-7	7-10	10-13	13-17	17-21	21-26	26-30	
$N_0$		271	442	516	316	218	113	77	39	
$N$		249.6	406.7	454.6	286.6	191.8	95.3	60.6	28.2	
$N_{cor}$		229.6	370.1	450.1	283.4	195.6	94.3	57.6	28.2	
$\sigma_{tot}/E_\nu$		0.357	0.341	0.335	0.327	0.302	0.285	0.269	0.258	
$\Delta_{stat}$		0.020	0.016	0.014	0.018	0.021	0.030	0.037	0.051	
$\Delta_{\Sigma sys}$		0.031	0.026	0.026	0.028	0.028	0.027	0.031	0.039	

Two methods were used to estimate neutrino spectra from the experimental data:

1. Estimation method based on quasi-elastic events.

For the selection of quasi-elastic events the criterion  $\nu = Ey < \nu_0 = 0.3$  GeV was used. With such value of  $\nu_0$  optimal signal/background ratio was reached, and a part of quasi-elastic interactions in selected events is sufficiently high  $\approx 60\%$  in the whole range of neutrino energy. Cross section of quasi-elastic interaction is well known [37],[38] and is practically constant at  $E_\nu > 3$  GeV, it's theoretical uncertainty is 5% [35] due to the uncertainty of the parameter  $M_A = 1.00 \pm 0.04$  GeV. A quasielastic sample has a significant contribution of resonance production, this gives an additional  $\approx 4\%$  error in the normalization of the spectra obtained by this method.

2. From the well-known formula of differential cross section for deep inelastic interaction one can obtain [36]

$$\lim_{y \rightarrow 0} \frac{1}{E} \frac{d\sigma}{dy} = \frac{G^2 M}{\pi} \int_0^1 dx F_2(x, Q^2 \rightarrow 0) = const. \quad (1)$$

Therefore

$$\lim_{y \rightarrow 0} \frac{1}{E_\nu} \frac{dN(E_i)}{dy} = const \cdot \Phi(E_\nu), \quad (2)$$

where  $\Phi(E_\nu)$  is the neutrino flux. When selecting events for spectrum estimation in this way, quasi-elastic and resonance events were excluded, for this purpose only region  $y > 1.67/E_\nu$  was under consideration. This limitation did not allow one to use this method in the energy region below 10 GeV.

Fig.9a shows the ratio of the spectrum, obtained by the first method to the spectrum from  $\pi, K$ -mesons (narrow rectangles), and the ratio of the spectrum obtained by the second method to that from  $\pi, K$ -mesons (wide rectangles).

The two above methods use different samples of neutrino events, therefore the obtained spectra errors are uncorrelated. Averaging these spectra together with those from  $\pi, K$ -mesons, the spectrum, used for the calculation of total cross sections was obtained; its ratio to the spectrum from  $\pi, K$ -mesons is shown on fig.9a by circles. The errors are within the lines limits. The similar notations were used on fig.9b for exposition with short decay base.

Spectrum  $\bar{\nu}_\mu$ , because of low statistics, was mainly defined by the spectrum from  $\pi, K$ -mesons.

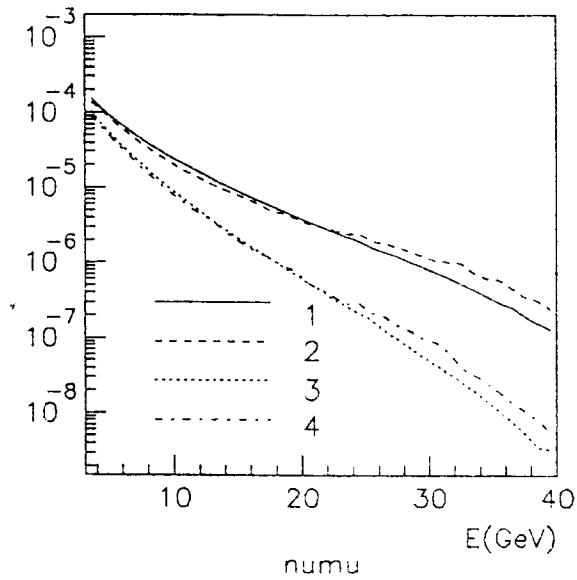


Fig. 7.  $\nu_\mu$  and  $\bar{\nu}_\mu$  fluxes for the exposition with the conventional geometry (1) and for the exposition with short decay base (2).

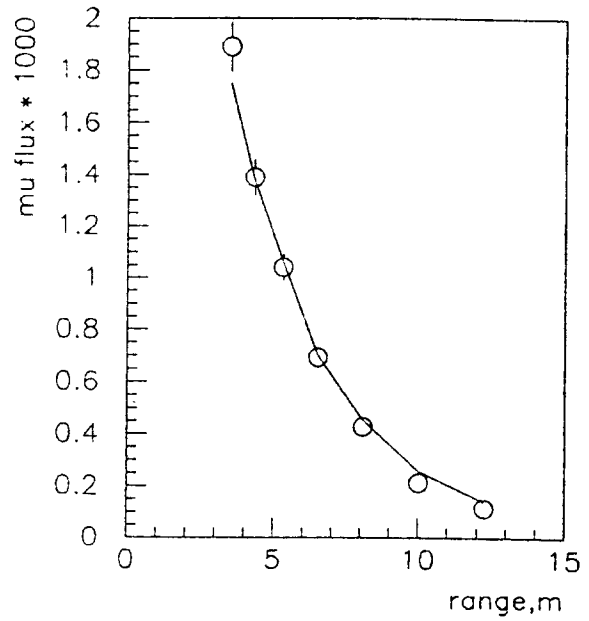


Fig. 8. The comparison of experimental muon fluxes in the gaps of muon filter with simulated ones.

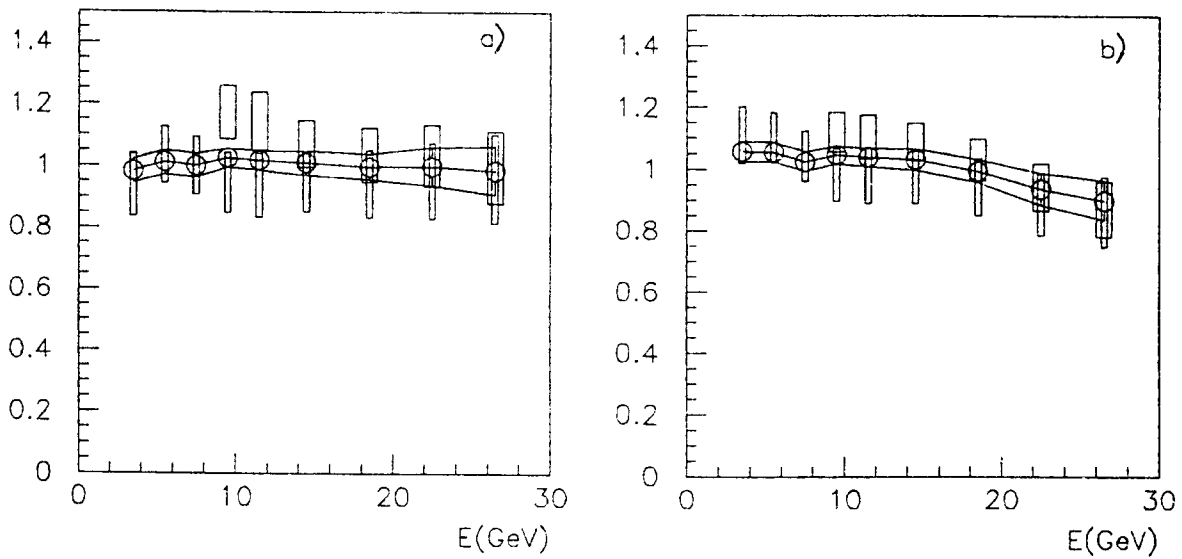


Fig. 9. The ratio of the spectrum, obtained from quasi-elastic events distribution, to the spectrum from  $\pi$ ,  $K$ -mesons (narrow rectangles), and the ratio of the spectrum, obtained from differential distribution  $d\sigma/dy$  to the spectrum from  $\pi$ ,  $K$ -mesons (wide rectangles). Resulting spectrum - circles. (a) - for the exposition with the conventional geometry, (b) - for the exposition with short decay base.

### 3.3. Calculation of $\sigma_{tot}$

Total cross section can be obtained by dividing the number of interactions in the detector by the product of the neutrino flux  $\Phi(E)$ , the number of nuclei per  $\text{cm}^2$  in the fiducial volume of the detector  $N^T$  and the detector efficiency (including the acceptance)  $\varepsilon(E)$

$$\sigma^{tot}(E) = \frac{N_{true}(E)}{N^T \cdot \Phi(E) \cdot \varepsilon(E)}. \quad (3)$$

We have the measured distribution  $N(E')$  instead of the true distribution  $N_{true}(E)$  because of finite resolution in variable  $E$

$$N(E') = \int dE S(E', E) \cdot N_{true}(E), \quad (4)$$

where  $S(E', E)$  is the transformation operator from the true distribution to the measured distribution. To solve the inverse problem and to calculate  $N_{true}(E)$  we must obtain the inverse transformation operator  $S^{-1}(E', E)$

$$N_{true}(E) = \int dE' S^{-1}(E', E) \cdot N(E'). \quad (5)$$

This method requires the use of complex procedure of the  $S$  regularization (described in [39],[40]), but here for the  $N_{true}(E)$  calculation we used a simpler method, described in Appendix. The distribution obtained by this procedure was marked in Tables 2 and 3 by  $N_{cor}$ . After substituting  $N_{cor}$  as  $N_{true}$  in (3) the energy dependence for the slope parameter of the total cross section  $\sigma_{tot}/E$  was defined (Tables 2 and 3).

When evaluating the systematic error of the total cross section slope  $\Delta_{\Sigma_{sys}}$  the contribution of the following uncertainties was taken into account:

- in the neutrino flux,
- in the value of the magnetic field  $\pm 1\%$ ,
- in the calculations of the hadron energy,
- in the efficiency of the neutrino event reconstruction,
- in the unsmearing procedure,
- 1% errors of proton beam intensity monitors.

## 4. Results and Discussion

The obtained dependences  $\sigma_{tot}/E$  were averaged over two expositions according to their errors (Table 4). These results are compared with the data published earlier (fig.10). Our measurements have the smallest errors in  $5 \text{ GeV} < E_\nu < 30 \text{ GeV}$  range and show, that  $\sigma_{tot}/E_\nu$  noticeably decreases with  $E_\nu$  increase from value  $\approx 0.8 \times 10^{-38} \text{ cm}^2$  for  $E_\nu=5 \text{ GeV}$  to that coinciding, within the limits of experimental accuracy, with the results, obtained for energies over 30 GeV. Note, that there is a good agreement with BNL experimental data [5] in the  $0.4 \text{ GeV} < E_\nu < 6 \text{ GeV}$  region, where experimentally defined  $\nu$  spectrum from quasi-elastic events in  $\nu n \rightarrow \mu^- p$  reaction was used. These data show, that the slope parameter still increases with further energy decrease.

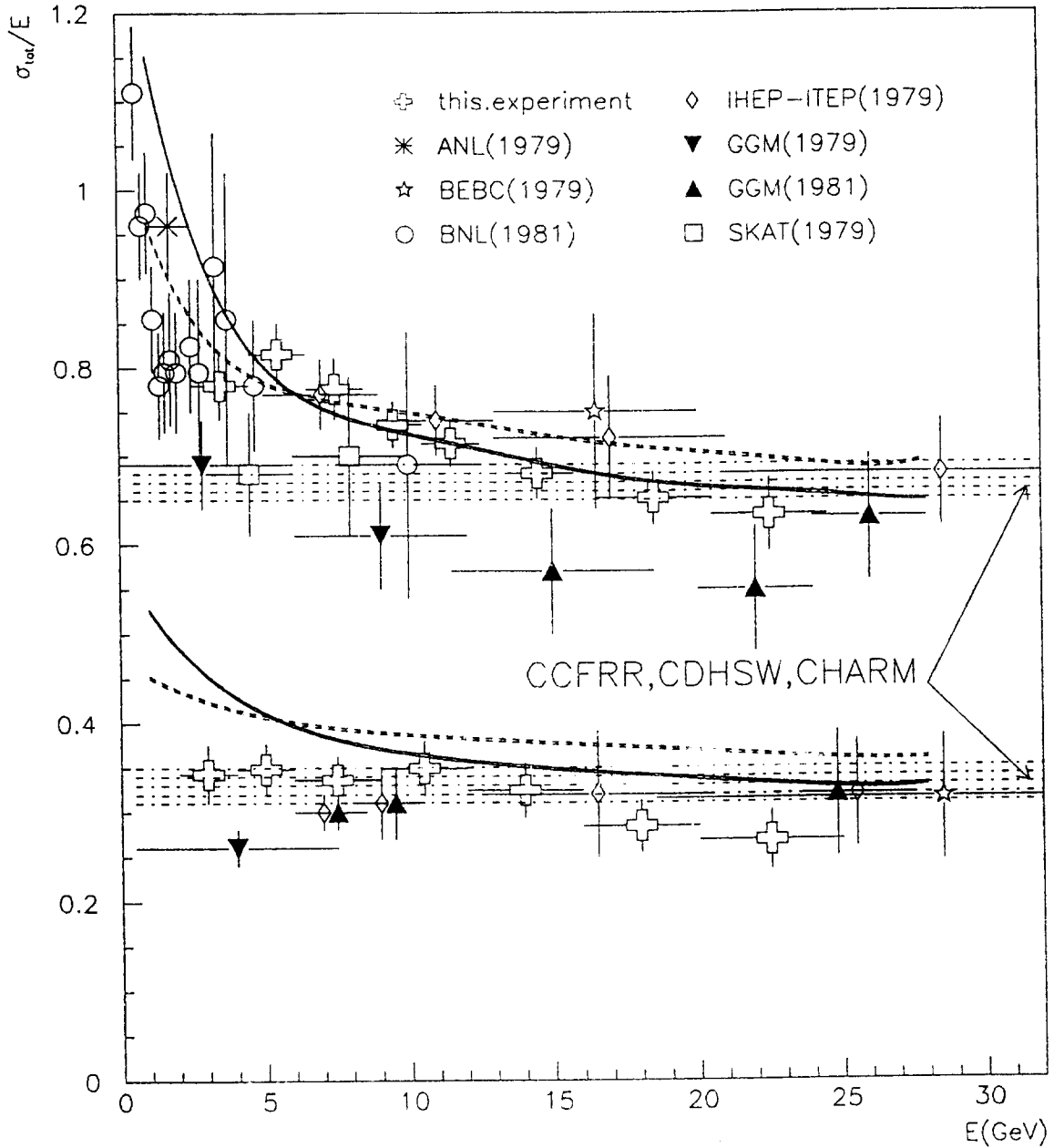


Fig. 10. The measured dependence of total cross section for  $\nu_\mu$  and  $\bar{\nu}_\mu$  interactions with nucleon versus neutrino energy in comparison with data from other experiments. Solid curve – calculation based on the GRV parameterization [45], dotted curve – KMRS [43].

On fig.10 the calculated dependences for total cross section versus energy are also represented as a sum of the total deep inelastic cross section and the cross section of quasi-elastic interaction ( according to [35]). The total deep inelastic cross section was calculated on the base of quark distributions, and their different parameterizations were taken from quark distribution library PDFLIB [41]. On fig.10 the calculation based on GRV parameterization [45] is represented by the solid curve, KMRS [43] by the dotted

Table 4. Neutrino and antineutrino total cross section ( $\sigma_{tot}/E_\nu \times 10^{-38} \text{ cm}^2 \text{ GeV}$ ) dependences versus energy obtained in a result of two expositions.

	neutrino								
$E_\nu$ [GeV]	3-5	5-7	7-9	9-11	11-13	13-17	17-21	21-25	25-30
$\sigma_{tot}/E_\nu$	0.780	0.816	0.776	0.735	0.714	0.680	0.652	0.633	0.609
$\Delta_{stat}$	0.016	0.013	0.014	0.016	0.018	0.015	0.020	0.024	0.031
$\Delta_{\Sigma syst}$	0.039	0.035	0.035	0.026	0.027	0.029	0.030	0.041	0.054
	antineutrino								
$E_\nu$ [GeV]	3-5	5-7	7-10	10-12	13-17	17-21	21-26	26-30	
$\sigma_{tot}/E_\nu$	0.343	0.348	0.336	0.349	0.324	0.284	0.268	0.278	
$\Delta_{stat}$	0.016	0.013	0.012	0.015	0.017	0.024	0.029	0.039	
$\Delta_{\Sigma syst}$	0.023	0.020	0.019	0.022	0.022	0.021	0.023	0.031	

curve. In calculations based on BEBC parameterization [42] and MT parameterization [44] the dependencies close to the results, based on KMRS parameterization were obtained. It should be noted, that the GRV parameterization gives quark distributions up to  $Q_{min}^2 = 0.25 \text{ GeV}^2$ , whilst the usage of KMRS and MT parameterization in the low energy region is not quite correct, since  $Q^2$  - evolution of structure functions is frozen at  $Q^2$  below  $Q_{min}^2 = 4 \text{ GeV}^2$ . The calculations showed, that in the 1-20 GeV energy region the total cross section slope parameter change was mainly stipulated by the quasi-elastic interaction contribution.

Table 5. The ratio of deep inelastic cross sections  $r_{inel} = \sigma_{inel}^\nu/\sigma_{inel}^{\bar{\nu}}$  and contribution of sea quarks  $R = \bar{q}/(\bar{q} + q)$  versus energy.

$E_\nu$ [GeV]	3-5	5-7	7-10	10-13	13-17	17-21	21-26	26-30
$r_{inel}$	0.395	0.379	0.411	0.468	0.459	0.419	0.408	0.466
$\Delta r_{inel}$	0.030	0.032	0.035	0.043	0.046	0.048	0.058	0.077
R	0.068	0.050	0.083	0.138	0.129	0.091	0.080	0.124
$\Delta R$	0.034	0.033	0.035	0.040	0.043	0.047	0.058	0.072

Table 5 presents the deep inelastic cross sections ratio  $r_{inel} = \sigma_{inel}^{\bar{\nu}}/\sigma_{inel}^\nu$  and sea quarks contribution

$$R = \frac{\bar{q}}{\bar{q} + q} = \frac{1}{2} \cdot \frac{3r_{inel} - 1}{r_{inel} + 1} \quad (6)$$

versus energy. After fitting over the whole energy range,  $r_{inel} = 0.420 \pm 0.016$  and  $\bar{q}/(\bar{q} + q) = 0.093 \pm 0.016$  were obtained. This is rather less, then for  $30 \text{ GeV} < E_\nu < 160 \text{ GeV}$ , where  $\bar{q}/(\bar{q} + q) = 0.154 \pm 0.012$  [16].

In conclusion we would like to thank the staff of the IHEP Proton Synchrotron and Experimental Facilities Divisions for efficient operation of proton beam. We wish to ex-



press our thanks to G.Conforto, director of the Institute for Physics of Urbino University (Italy), who placed at our disposal the computer facility for experimental data processing and simulations, F.Martilli, P.Dominichi and other collaborators for repeated kind assistance in the work.

## References

- [1] MacFarlane D.B. et al.//Z. Phys., C26, 1 (1984).
- [2] Berge P. et al.//Z. Phys., C35, 443 (1987).
- [3] Allaby J.V. et al.//Z. Phys. C38, 403 (1988).
- [4] Baltay C. et al.//Phys. Rev. Lett., 44, 916 (1980).
- [5] Baker N.I. et al.//Phys. Rev., D25, 617 (1982).
- [6] Eichten T. et al.//Phys. Lett., 46B, 274 (1973).
- [7] Erriquez O. et al.//Phys. Lett., 80B, 309 (1979).
- [8] Ciampolino S. et al.//Phys. Lett., 84B, 281 (1979).
- [9] Morfin J.G. et al.//Phys. Lett., 101B, 235 (1981).
- [10] Colley D.C. – Preprint DPhPE 79-12 (1979).
- [11] Baranov D.S. et al.//Phys. Lett., 81B, 255 (1979).
- [12] Vovenko A.S. et al.//Yad. Fiz., 30, 1014 (1979).
- [13] Barish S.J. et al.//Phys. Rev., D19, 2521 (1979).
- [14] Erriquez O. et al.//Phys. Lett., 80B, 309 (1979).
- [15] Barabash L.S. et al. - In: Proceed. of Intern. Conf. Neutrino-82, 1982, v.2, p. 249.
- [16] Baratov D.G. et al. - Preprint IHEP 76-84, Serpukhov, 1976;  
Baratov D.G. et al. - Preprint IHEP 76-87, Serpukhov, 1976.
- [17] Bugorsky A.P. et al.//NIM, 146, (1977), p. 367.
- [18] Bozhko N.I. et al.//NIM, A243 (1986), p. 388.
- [19] Bozhko N.I. et al. Pribory i Tekhnika Eksperimenta, N. 2, (1985), p. 57.
- [20] Brusin M.Yu. et al. - In the book: VII Workshop on Neutrino Detector IHEP-JINR, Dubna, 1986, p. 41.

- [21] Anikeev V.B. et al. - In the book: VIII Workshop on Neutrino Detector IHEP-JINR, Dubna, 1988, p. 120.
- [22] Bunyatov S.O. et al. - In the book: VII Workshop on Neutrino Detector IHEP-JINR, Dubna, 1986, p. 51.
- [23] Bozhko N.I. et al. - Preprint IHEP 91-138, Protvino, 1991.
- [24] Anikeev V.B. et al. - Preprint IHEP 93-28, Protvino, 1993.
- [25] Bozhko N.I. et al.//Yad. Fiz., 31, 1246 (1980); Yad. Fiz, 31, 1494 (1980).
- [26] Akerlof K. et al. - Preprint IHEP 77-86, Serpukhov, 1977.
- [27] Bugorsky A.P. et al. - Preprint IHEP 72-72, Serpukhov, 1972.
- [28] Bugorsky A.P. et al. - Preprint IHEP 78-116, Serpukhov, 1978.
- [29] Belkov A.A. et al. - Preprint IHEP 82-99, Serpukhov, 1982.
- [30] Kirsanov M.M., Calculations of neutrino spectra with a program based on GEANT library. - Preprint IHEP, to be published.
- [31] GEANT manual, CERN Program Library Long Writeup W5013, Copyright CERN, Geneva, 1993.
- [32] Kravtsov V.I. et al. - In the book: VIII Workshop on Neutrino Detector IHEP-JINR Dubna, 1988, p. 109.
- [33] Field R.D., Feynman R.P.//Phys. Rev, D15, 2590 (1977).
- [34] Rein D., Sehgal L.M.//Nucl. Phys., B223, 29 (1983).
- [35] S.V.Belikov et al. - Preprint IHEP 83-156, Serpukhov, 1983.
- [36] Auchincloss P.S. et al.//Z. Phys., 18, 411.
- [37] Grabosh G. et al. - Preprint IHEP 86-221, Protvino, 1986.
- [38] Belikov S.V. et al. - Preprint IHEP 81-62, Serpukhov, 1981.
- [39] Anykeyev V.B., Zhigunov V.P.//Phys. Part. Nucl., 24, 424 (1993).
- [40] Anykeyev V.B., Spiridonov A.A., Zhigunov V.P.//Nucl. Instr. Meth., A303, 350 (1991).
- [41] Plothow-Besch Y. - In: Proceeding of the 3rd Workshop on Detector and Event Simulation in High Energy Physics, Amsterdam, 1991.
- [42] Buras A.J., Gaemers K.J.F.//Nucl. Phys. B132, 219 (1978).

- [43] Kwiecinski J. et al.//Phys. Rev. D42, 3645 (1990).  
 [44] Morfin J.G., Tung W.K.//Z.Phys., C52, 13 (1991).  
 [45] Gluck M. et al.//Z. für Physik, 48, 411 (1992).  
 [46] Allaby J.V. et al. – Preprint CERN-EP/87-225 (1987).

Received March 16, 1995

## Appendix

### Method for the Inverse Problem Solution in Calculating the Differential Cross Section

Let the true distribution over the variable  $\xi$  be  $S(\xi) = \varphi(\xi) \cdot d\sigma(\xi)/d\xi$ .

Because of the measurement errors, instead of the true distribution as a result of the experiment we obtain the distribution<sup>1</sup>

$$\dot{S}(\xi) = c \int d\xi' K(\xi'|\xi) E(\xi) S(\xi), \quad (7)$$

where  $E(\xi)$  is the detector efficiency,  $K(\xi|\xi')$  is the probability to obtain the value  $\xi'$  instead of the true value  $\xi$  as the result of measurement.

$A_n(\xi)$  is the probability for event to enter the  $n$ -th bin of the histogram and can be written as

$$A_n(\xi) = \int_{\xi_n}^{\xi_{n+1}} d\xi' K(\xi'|\xi) E(\xi), \quad (8)$$

and the mean value for the events number in the  $n$ -th bin is  $\bar{Y}_n = \int d\xi A_n(\xi) S(\xi)$ .

On the base of the model or *a priori* information the distribution  $S_0(\xi)$  is chosen as an approximation of the true distribution  $S(\xi)$ . Based on this distribution  $S_0(\xi)$  with the program simulating the measurement process in the experiment the distribution of simulated events is calculated

$$Y_n^{MC} = \int d\xi A_n(\xi) S_0(\xi)$$

and the probability for the event in the  $n$ -th bin of the histogram to have true value  $\xi$  is

$$A'_n(\xi) = \frac{1}{Y_n^{MC}} \cdot A_n(\xi) S_0(\xi). \quad (9)$$

As an estimate of the true distribution  $S(\xi)$  we can use (10)

---

<sup>1</sup>For a sake of simplicity we consider all measured events included in the experimental histogram.

$$\check{S}(\xi) = \sum_n Y_n A'_n(\xi).$$

It is clear that if we use as a model approach  $S_0(\xi)$ , the distribution which is proportional to the true distribution  $\cdot kS(\xi)$  then the estimate  $\check{S}(\xi)$  from (10) will give us the true distribution  $S(\xi)$

$$\overline{\check{S}(\xi)} = \overline{\sum_n Y_n A'_n(\xi)} = \sum_n \frac{Y_n A_n(\xi) k S(\xi)}{\int d\xi A_n(\xi) k S(\xi)} = S(\xi) \sum_n A_n(\xi) \approx S(\xi).$$

If the width of distributions  $A(\xi)$  is negligibly small, then the estimate  $\check{S}(\xi)$  from (8) can be reduced to the frequently used estimate provided by the correcting factors method

$$\int_{\xi_n}^{\xi_{n+1}} \check{S}(\xi_n) = \int_{\xi_n}^{\xi_{n+1}} d\xi \sum_n Y_n A'_n(\xi) \approx \frac{Y_n \cdot S_0(\xi_n) \cdot \Delta\xi_n}{Y_n^{MC}}.$$

The approximate  $\check{S}(\xi)$  explicitly depends on the model distribution  $S_0(\xi)$ , and varying it in the allowable limits we will obtain the error in the calculation of the true distribution estimate with the above procedure.

Assuming the function  $\varphi(\xi)$  to be known, one can calculate the cross section  $d\sigma/d\xi$  from the obtained estimate  $\check{S}(\xi)$ .

В.Б.Аникеев и др.


Определение полных сечений нейтрино и антинейтрино на диклозе в области 3-30 ГэВ на Нейтринном Детекторе ИФВЭ-ОИЯИ.

Оригинал-макет подготовлен с помощью системы L<sup>A</sup>T<sub>E</sub>X.

Редактор Е.Н.Горина.

Технический редактор Н.В.Орлова.

---

Подписано к печати 16.03.1995 г.  Формат 60 × 84/8.      Офсетная печать.  
Печ.л. 2.25.    Уч.-изд.л. 1.73.    Тираж 250.    Заказ 289.    Индекс 3649.  
ЛР №020498 06.04.1992.

---

ГНЦ РФ, Институт физики высоких энергий  
142284, Протвино Московской обл.

